*Acta metall.* Vol. 36, No. 8, pp. 2335–2347, 1988
Printed in Great Britain

0001-6160/88 $3.00 + 0.00
Pergamon Press plc

# CONTINUOUS GROWTH MODEL FOR INTERFACE MOTION DURING ALLOY SOLIDIFICATION

**MICHAEL J. AZIZ[1] and THEODORE KAPLAN[2]**

[1]Division of Applied Sciences, Harvard University, Cambridge, MA 02138, U.S.A. and
[2]Solid State Division, Oak Ridge National Laboratory, Oak Ridge, TN 37831, U.S.A.

(*Received* 27 *July* 1987)

**Abstract**—A model is developed that predicts the steady state velocity of a planar interface and the chemical composition of the growing phase in terms of the interface temperature and the composition of the parent phase at the interface. The model is applied to solidification of a two-component melt. Solute partitioning is treated by a previously developed continuous growth model for solute trapping. The interface velocity is found by generalizing the driving force in a velocity-vs-driving force function used for solidification of one-component melts. Two different ways of generalizing the driving force are used, with and without the inclusion of a "solute drag" term. Predictions are made both with and without solute drag for an ideal solution and for Ag–Cu, a simple eutectic system in which the terminal phases have the same crystal structure. In both cases, a transition from diffusion-controlled to diffusionless solidification and a falling interface temperature occur as the interface velocity increases. In the model without solute drag, significantly less interfacial undercooling is predicted than in the model with solute drag. The relationship to previous theoretical work, especially to the continuum treatments of Baker and Cahn, and to pertinent experiments is discussed.

**Résumé**—Nous développons un modèle qui prédit la vitesse, à l'état stationnaire, d'une interface plane et la composition chimique de la phase qui croît, en fonction de la température de l'interface et de la composition de la phase mère à l'interface. Nous appliquons ce modèle à la solidification d'un bain à deux constituants. Nous traitons le partage du soluté à l'aide d'un modèle de croissance continue que nous avions développé auparavant pour le piégeage des solutés. Nous trouvons la vitesse de l'interface en généralisant la force motrice dans une fonction vitesse/force motrice que l'on utilise pour la solidification des bains à un seul constituant. Nous généralisons la force motrice de deux façons différentes, en incluant ou non un terme de "traînage de soluté". Nous établissons des prédictions, avec et sans traînage de soluté, dans le cas d'une solution idéale et pour le système Ag–Cu qui est un eutectique simple où les solutions solides terminales ont la même structure cristalline. Dans les deux cas, lorsque la vitesse de l'interface augmente, il apparaît une transition dans le mode de solidification (mode régi par la diffusion → mode sans diffusion) et une chute de la température interfaciale. Nous prédisons dans le modèle sans traînage de soluté une surfusion interfaciale nettement moins prononcée que dans le modèle avec traînage de soluté. Nous discutons les relations qui existent entre cette étude et un travail théorique antérieur, en particulier les traitements en milieu continu dûs à Baker et à Cahn.

**Zusammenfassung**—Ein Modell wird entwickelt, welches die stationäre Geschwindigkeit einer ebenen Grenzfläche und die chemische Zusammensetzung der wachsenden Phase anhand der Grenzflächentemperatur und der Zusammensetzung der Mutterphase an der Grenzfläche voraussagt. Dieses Modell wird auf die Erstarrung einer zweikomponentigen Schmelze angewendet. Die Aufteilung des gelösten Stoffes wird mit einem früher behandelten kontinuierlichen Wachstumsmodell für das Einschließen des gelösten Stoffes behandelt. Die Grenzflächengeschwindigkeit ergibt sich, indem die treibende Kraft in eine Funktion Geschwindigkeit über treibender Kraft, die für die Erstarrung einer einkomponentigen Schmelze benutzt worden ist, verallgemeinert wird. Zur Verallgemeinerung werden zwei verschiedene Wege benutzt, mit und ohne Berücksichtigung eines Terms, der eine Reibungsspannung durch den gelösten Stoff beschreibt. Für beide Fälle werden Voraussagen abgeleitet für eine ideale Lösung und für Au–Cu, einem einfachen eutektischen System, bei dem die Endphasen dieselbe Kristallstruktur besitzen. In beiden Fällen treten ein Übergang von der diffusionsbestimmten zur diffusionslosen Erstarrung und ein Abfall der Erstarrungstenperatur auf, wenn die Geschwindigkeit der Grenzfläche größer wird. Im Modell ohne Reibungsterm ergibt sich eine beträchtlich geringere Unterkühlung an der Grenzfläche als mit Reibungsterm. Der Zusammenhang mit früheren theoretischen Untersuchungen, insbesondere den Kontinuumsbehandlungen von Baker und Cahn und mit den zugehörigen Experimenten wird diskutiert.

## 1. INTRODUCTION

Conventional kinetic descriptions of solidification treat the near-equilibrium limit. This is the case in which transport of heat or solute through the bulk of one or both of the phases separated by an interface is the rate-limiting step in the process and is subject to local equilibrium boundary conditions at the interface. In this limit, crystal growth occurs slowly enough that, although long-range transport may be too slow to maintain thermal or compositional equilibrium throughout the bulk of either phase, short-range transport across the interface may still be sufficiently rapid to effect interequilibration among the atoms comprising the liquid monolayer and the solid monolayer adjacent to the interface. This

assumption implies that, given a liquid composition at the interface, the solid grows at the equilibrium temperature with the equilibrium composition, given by the liquidus and solidus on the equilibrium phase diagram [1].

Rapid solidification experiments have now attained a regime of crystal growth speed where the deviations from local equilibrium are very important, in which interface motion cannot be thought of as heat-flow or diffusion limited. These experiments provide an opportunity to study the interface reaction kinetics in high-mobility systems. The formation of metallic glasses [2] and other metastable metallic and semiconducting phases [3] in the presence of rapidly moving crystal-melt interfaces demonstrates significant undercooling of the crystal–melt interface during rapid crystal growth. Splat-quenching of molten metallic alloys [4] and rapid regrowth from pulsed-laser-induced melting of doped semiconductors [5, 6] have produced suppressed solute partitioning, where the partition coefficient $k$ (the ratio of the solute concentration in the growing solid to that in the liquid at the interface) deviates from its equilibrium value $k_e$ (the ratio of the equilibrium solidus to liquidus compositions on the phase diagram) and approaches unity at high interface speeds. Indeed, it has been demonstrated that in alloys with retrograde solid solubility the chemical potential of the minor element increases during rapid solidification [4]. The discovery of this phenomenon, termed "solute trapping",† ruled out both local equilibrium and the idea that the alloy components might act independently during rapid solidification [7]. A number of kinetic models [8–17] have been proposed to account for solute trapping and related phenomena observed during rapid phase transformations.

Two questions must be addressed by models for plane-front interface motion during a phase transformation in a two-component system. Given local conditions at the interface (e.g. temperature, composition, pressure), they should predict (1) the composition of the growing phase and (2) the interface velocity. The boundary conditions discussed above are provided by answers to these questions. Combined with equations for long range transport that connect the interface conditions to the ambient, externally controllable conditions, they can yield predictive capability for materials processing.

The measured velocity and orientation dependence of $k$ during solidification of Bi-doped Si is successfully accounted for by the dilute solution limit of the continuous growth model (CGM) [18, 19]. Thus the CGM seems to answer the former question. To propose an answer to the latter question, the dilute solution CGM has been extended to concentrated solutions and combined with a dissipation-theory treatment of crystal growth [15], which is an outgrowth of the solute-drag theory of Hillert and Sundman [12]. Only indirect comparison with experiment has been possible in this case [20], but so far the results are promising. The CGM is consistent with the experimental observations of which we are aware. It predicts solidification under local equilibrium conditions at small interface velocities, and partitionless solidification and large undercoolings at high velocities. The model treats alloy solidification as a superposition at the interface of two distinct reactions: crystallization via the advance of the interface across a monolayer of liquid alloy, and solute–solvent redistribution via interdiffusion of the two species across the interface. The rate of each reaction is written in terms of its driving force and its mobility using chemical rate theory [21].

In the next section this model is developed more fully. The differences are demonstrated between versions of the model that neglect and allow for an effect on the interface velocity due to free energy dissipation from solute drag. There is nothing specific to solidification in the model; it may equally well be applied to appropriate solid-state transformations, with proper choices for the values of the kinetic parameters. In the third section, a comparison is made with the continuum models of Baker and Cahn. The versions of our model with and without solute drag are shown to be limiting cases of the continuum model. In the final section, solutions are presented for binary alloy solidification, for both versions of the model, for an ideal solution and for a simple eutectic system in which the terminal phases have the same crystal structure.

The symbols used in the paper are defined where they first appear; for convenience they are also assembled with their definitions in Table 1.

## 2. THE MODEL

Consider a two-phase system composed of A (solvent) and B (solute) atoms. A liquid and a crystal are separated by a planar interface moving into the liquid at a steady-state velocity $v$ ($v \geqslant 0$) with respect to the crystal lattice. Assume for the sake of simplicity that A and B in the solid and in the liquid have the same atomic volume $\Omega$. The temperature of the interface is $T$; the mole fraction of B in the solid is $X_S$ and that in the liquid *adjacent to the interface* is $X_L$. The numbers of A and B atoms per unit area per unit time that are incorporated into the crystal, $J_A$ and $J_B$ respectively, are given by

$$J_A = (1 - X_S)v/\Omega, \tag{1a}$$

$$J_B = X_S v/\Omega. \tag{1b}$$

$J_A$ and $J_B$ are physical fluxes of atoms across any plane parallel to the interface in a coordinate system

†The term "solute trapping" was originally applied only to situations where the chemical potential of the solute increases during solidification. It is now commonly used in any situation where the partition coefficient deviates toward unity from its equilibrium value, independent of the sign of the change in chemical potential (which often is not determined experimentally).

Table 1. Symbols and definitions

| | |
|---|---|
| $A$ | solvent species |
| $B$ | solute species |
| $D_i$ | interdiffusion coefficient across interface |
| $E$ | standard chemical potential |
| $F_A$ | conjugate driving force for $J_A$ |
| $F_B$ | conjugate driving force for $J_B$ |
| $F_C$ | conjugate driving force for $J_C$ |
| $F_D$ | conjugate driving force for $J_D$ |
| $f$ | geometric factor for interdiffusion |
| $\dot{G}$ | free energy dissipation per unit area of interface per unit time |
| $\Delta G_C$ | crystallization free energy, equation (20) |
| $\Delta G_D$ | solute drag free energy, equation (21) |
| $\Delta G_{DF}$ | driving free energy, equation (19) |
| $J_A$ | flux of A across interface, equation (1a) |
| $J_A^D$ | diffusive flux of A, equation (2a) |
| $J_B$ | flux of B across interface, equation (1b) |
| $J_B^D$ | diffusive flux of B, equation (2b) |
| $J_C$ | crystallization flux, equation (4) |
| $J_D$ | diffusive flux, equation (3) |
| $j_d$ | generalized diffusive flux in continuum model |
| $k$ | partition coefficient of B, equation (11) |
| $k_A$ | partition coefficient of A, $(1-X_S)/(1-X_L)$ |
| $k_e$ | equilibrium partition coefficient of B |
| $k_e^A$ | equilibrium partition coefficient of A |
| $k_0$ | dilute solution limit of $k_e$ |
| $L_{ij}$ | phenomenological mobility matrix |
| $M$ | interface mobility |
| $P$ | force on interface per unit area |
| $Q_D$ | activation energy for redistribution |
| $R$ | gas constant |
| $\dot{S}$ | irreversible entropy production per unit area of interface per unit time |
| $T$ | interface temperature |
| $T_0$ | temperature at which phases of equal composition have equal free energy |
| $v$ | interface speed |
| $v_D$ | speed of solute-solvent redistribution at infinite driving force |
| $v_0$ | speed of crystallization at infinite driving force |
| $X$ | mole fraction of solute |
| $X_L$ | mole fraction of solute in liquid at interface |
| $X_S$ | mole fraction of solute in solid at interface |
| $y$ | position in direction normal to interface |
| $\delta$ | width of interface |
| $\kappa_e$ | partitioning parameter, $\exp[(\Delta\mu_A' - \Delta\mu_B')/RT]$ |
| $\lambda$ | interatomic distance |
| $\mu$ | chemical potential |
| $\Delta\mu_A$ | $\mu_A$ in solid minus $\mu_A$ in liquid at interface |
| $\Delta\mu_B$ | $\mu_B$ in solid minus $\mu_B$ in liquid at interface |
| $\mu^\circ$ | standard chemical potential |
| $\mu'$ | chemical potential minus contribution from ideal mixing entropy, equation (8) |
| $\Delta\mu_A'$ | $\mu_A'$ in solid minus $\mu_A'$ in liquid at interface |
| $\Delta\mu_B'$ | $\mu_B'$ in solid minus $\mu_B'$ in liquid at interface |
| $\nu$ | attempt frequency for surmounting barrier |
| $\Omega$ | atomic volume |

fixed on the interface, but not in a coordinate system fixed on the lattice. The "diffusive" fluxes $J_A^D$ and $J_B^D$ are the differences between the actual fluxes and what the fluxes would be if the solid grew with the composition of the liquid at the interface. They are defined by

$$J_A^D = (1 - X_L)v/\Omega - J_A, \tag{2a}$$

$$J_B^D = X_L v/\Omega - J_B. \tag{2b}$$

Combining (1) and (2), we find

$$-J_A^D = (X_L - X_S)v/\Omega = J_B^D \equiv J_D. \tag{3}$$

We call $J_D$ the diffusive flux. It is this quantity that represents a physical flux of atoms in a coordinate system fixed on the lattice across a particular plane (the plane immediately adjacent to the interface in the liquid).

The total number of atoms per unit area per unit time that are incorporated into the crystal, called the crystallization flux $J_C$, is given by

$$J_C = v/\Omega; \tag{4}$$

it is the sum of $J_A$ and $J_B$. We refer the reader to the review by Baker and Cahn [1] for more on the choices of fluxes and driving forces in the alloy solidification problem.

### 2.1. *Solute partitioning*

The diffusive flux is expressed phenomenologically in terms of the driving force for solute–solvent redistribution and the kinetic rate constant, or mobility, for the process. This can be done very simply for a dilute solution of B in A:

$$J_D = (v_D/\Omega)(X_S - k_e X_L), \tag{5}$$

where $X_S - k_e X_L$ is a measure of the deviation from equilibrium and $v_D/\Omega$ is a kinetic constant relating the rate of return to equilibrium to the deviation from equilibrium. The characteristic velocity for the redistribution reaction $v_D$ can be identified within the framework of chemical rate theory as the maximum speed of interdiffusion at infinite driving force (i.e. when $k_e \to 0$). This diffusive speed is the ratio of $D_i$, the coefficient for interdiffusion across the interface, to the interatomic spacing $\lambda$. For concentrated solutions, one assumes a reaction from an initial state (of a B in the solid adjacent to an A in the liquid) over a barrier to a final state (where the two atoms have exchanged positions), as depicted in Fig. 1. In this case the forward reaction is written

$$J_D^+ = (f\nu\lambda)(X_S/\Omega)(1 - X_L)\exp\{-Q_D/RT\}, \tag{6}$$

where $f$ is a geometric factor, $\nu$ is an attempt frequency (which is on the order of an atomic vibrational frequency [22]), $Q_D$ is the activation barrier for interdiffusion across the interface, and $R$ is the gas constant. The second and third factors in (6) reflect the fact that the forward rate of A–B exchange is proportional to the concentration of B in the solid and the concentration of A in the liquid at the interface. The final factor is the fraction of attempted

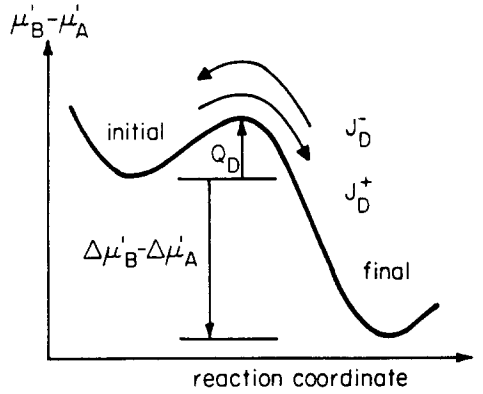


Fig. 1. Reaction coordinate diagram for solute-solvent redistribution reaction. Initial state: B in solid, A in liquid. Final State: B in liquid, A in solid.

interchanges that are successful. The rate of the reverse reaction is

$$J_D^- = (f\nu\lambda)(X_L/\Omega)(1-X_S) \times \exp\{-[Q_D + (\Delta\mu'_B - \Delta\mu'_A)]/RT\}, \quad (7)$$

where the final factor, the fraction of successful attempts, is again a Boltzmann factor in the barrier height. We use the convention that differences in quantities across the interface, expressed by the symbol $\Delta$, are the values of these quantities in the solid at the interface minus those in the liquid at the interface. The redistribution potential, $\mu'$, is the actual chemical potential minus the contribution from the ideal mixing entropy:

$$\mu'(X, T) \equiv \mu(X, T) - RT \ln X. \quad (8)$$

The redistribution potential can be thought of as very similar to the standard chemical potential $\mu$, except that it includes any composition dependence of the activity coefficient. The reason for the use of the redistribution potential rather than the internal energy or the actual chemical potential is that we include any local entropy effects in weighting the rates of individual atomic jumps, whereas the ideal mixing entropy is already accounted for by the $X_L(1-X_S)$ and $X_S(1-X_L)$ factors in equations (6) and (7). If these effects are included, the net flux vanishes in equilibrium (when $\Delta\mu_A = 0 = \Delta\mu_B$).

The net diffusive flux is then the difference between the forward and reverse reactions:†

$$J_D = J_D^+ - J_D = [v_D/\Omega][X_S(1-X_L) - \kappa_e X_L(1-X_S)], \quad (9)$$

where the diffusive speed is $v_D \equiv (f\nu\lambda)\exp[-Q_D/RT]$ and the partitioning parameter $\kappa_e(X_L, X_S, T) \equiv \exp[-(\Delta\mu'_B - \Delta\mu'_A)/RT]$ is a measure of the driving force for redistribution.

The departure of $X_S$ and $X_L$ from their equilibrium values during rapid interface motion in concentrated solutions necessitates the generalization of $k_e$ to $\kappa_e$. If $\kappa_e \ll 1$ the B atoms in the solid can lower their energies (actually, their $\mu'$) significantly by exchanging places with A atoms in the liquid; if $\kappa_e \gg 1$ the A atoms in the solid can lower their energies significantly by exchanging places with B atoms in the liquid, and if $\kappa_e \approx 1$ the energy change upon atomic redistribution is small. Note that if individual solute and solvent atoms in the liquid both want equally badly to transfer to the solid we still have $\kappa_e \approx 1$; very little redistribution across the interface results (rather we will tend to have rapid partitionless crystal growth, as will be reflected in the rate equation governing the crystal growth reaction). Typically $\kappa_e < 1$ and the solute prefers the liquid phase. Note that $\kappa_e$ is defined at all temperatures and solid and liquid compositions, but when $X_S$ is on the equilibrium solidus and $X_L$ is on the equilibrium liquidus $\kappa_e$ reduces to $k_e/k_e^A$, the ratio of the equilibrium partition coefficients of B and A (the partition coefficient of A is defined by $k^A \equiv (1-X_S)/(1-X_L)$). In addition, as long as Henry's law holds, then even far from equilibrium $\kappa_e(X_L, X_S, T) = k_e(T)/k_e^A(T)$. For dilute solutions of B in A, $k^A \approx 1$ and $\kappa_e$ further reduces to $k_e(T)$.

Combining (3) and (9), we have

$$(X_L - X_S)(v/v_D) = X_S(1-X_L) - \kappa_e X_L(1-X_S), \quad (10)$$

which can be solved for the partition coefficient:

$$k(v) = \frac{X_S}{X_L} = \frac{\dfrac{v}{v_D} + \kappa_e}{\dfrac{v}{v_D} + 1 - (1-\kappa_e)X_L}. \quad (11)$$

In the dilute solution limit, this result reduces to

$$k(v) = [(v/v_D) + k_e]/[(v/v_D) + 1], \quad (12)$$

which was derived by Brice [10] by combining equations similar to (3) and (5). We find a transition from equilibrium partitioning ($k \to k_e$) to complete solute trapping ($k \to 1$) as the interface speed surpasses the maximum speed of redistribution.

Imagine keeping the driving force for redistribution at a large but constant level while increasing the driving force for solidification. According to (9), $J_D$ will remain essentially constant. Simultaneously, $J_A$ and $J_B$ increase and approach values much greater in magnitude than $J_D$. Then according to (2), the *ratio* of $J_A$ or $J_B$ to the value it would have if solidification were partitionless approaches unity as the interface velocity increases. Although the instantaneous diffusive flux does not decrease, the amount of time that such a flux has in order to effect redistribution of a volume element of material at the interface diminishes with increasing interface speed. This is the basis for suppressed partitioning in this model. That $J_A$ and $J_B$ can very much exceed $J_D$ when

†This equation and several others appear in Ref. [15] with minus sign errors due to inconsistent sign conventions in the definitions of some quantities.

all pertinent driving forces increase without limit is a consequence of the Turnbull collision-limited growth model for solidification of simple molecular systems [23, 24]. However, even in systems where the mobilities for the crystallization and redistribution reactions are equal and hence $v \leqslant v_D$, partially suppressed partitioning will still follow from (11).

*2.2. Interface velocity*

We assume a local law in which all of the driving free energy, evaluated across the interface, is dissipated at the interface, the site of the reaction, with no coupling to driving forces and dissipation in the bulk. It is a simple matter then to calculate the decrease in free energy of the system, or equivalently, the increase in entropy of the universe, over the course of the reaction. This is done simply by examining the compositions and the chemical potentials adjacent to the reaction zone (i.e. the interface itself) in the final and initial phases. We will postulate a relationship between the interface velocity and the free energy dissipation.

We model the overall reaction as a superposition of two distinct irreversible processes. The fluxes associated with the pair of individual reactions can be either those of the individual species $J_A$ and $J_B$, or the crystallization and diffusive fluxes $J_C$ and $J_D$. The latter pair can be related to the former by a change of basis, as discussed by Baker and Cahn [1]. In both cases the formalism of irreversible thermodynamics [25] has been used, in which coupled generalized fluxes $J_i$ and their conjugate driving forces $F_i$ are related by a mobility matrix of phenomenological coefficients: $J_i = \Sigma L_{ij} F_j$. The sum is over whichever pair of independent fluxes we choose to describe the problem. Linear force–flux laws of this form are usually assumed in irreversible thermodynamics; they are *not* necessary for the results that we obtain in this work.

The rate $\dot{S}$ of irreversible entropy production per unit area of interface is, under conditions of constant temperature and pressure, simply equal to the decrease in the free energy of the system and is then given by

$$\Sigma J_i F_i = T\dot{S} = -\dot{G}, \tag{13}$$

where $\dot{G}$ is the Gibbs free energy dissipated by irreversible processes per unit area of interface. If we choose to describe the transformation in terms of $J_A$ and $J_B$, we evaluate the dissipation of free energy by examining the chemical potentials and compositions in the final and initial phases:

$$\dot{G} = J_A \Delta\mu_A + J_B \Delta\mu_B. \tag{14}$$

For (13) and (14) to hold for all independent variations of $J_A$ and $J_B$ we must have $F_A = -\Delta\mu_A$ and $F_B = -\Delta\mu_B$ [26, 27]. We are also assuming that we can neglect the free energy dissipated by other irreversible processes, such as heat flow, at the interface.

We now make a linear transformation to a more convenient reference frame. In the new basis, the fluxes are given by

$$J_C = J_A + J_B, \tag{15a}$$

$$J_D = X_L J_A - (1 - X_L) J_B; \tag{15b}$$

and the conjugate driving forces by

$$F_C = (1 - X_L) F_A + X_L F_B, \tag{16a}$$

$$F_D = F_A - F_B. \tag{16b}$$

It seems that phase transformations at an atomically sharp interface can be better understood in simple terms in this reference frame. It has already been demonstrated experimentally [28] that the results of dilute solute partitioning experiments are quite well described by a simple relationship between $J_D$ and $F_D$, equation (9). Note that (15b) is equivalent to (3). For the purposes of the linear transformation (equations 15 and 16) we have expressed the entire transformation using $X_L$ as the only parameter. The above transformation was chosen to leave the entropy production invariant, i.e. (13) remains valid in the new reference frame:

$$T\dot{S} = J_C F_C + J_D F_D, \tag{17}$$

as can be seen by inserting (15) and (16) into (17). To express (17) in terms of free energy per mole of material solidified we multiply each term in (17) by $-\Omega/v$, yielding

$$\Delta G_{DF}(v) = \Delta G_C(v) + \Delta G_D(v). \tag{18}$$

We learn from this equation that in the steady state the phase transformation is doing no work on the surroundings and therefore the free energy difference between the starting phase and the final phase must be entirely dissipated by irreversible processes during the reaction. As suggested by Hillert and Sundman [29] and as demonstrated in the next section of this paper, we can rephase this statement by dividing each free energy term by the molar volume. We then say that the sum of the forces per unit area on an interface moving at constant velocity is zero. The left-hand side of (18) is evaluated using (1) and (14):

$$\Delta G_{DF} = X_S \Delta\mu_B + (1 - X_S)\Delta\mu_A. \tag{19}$$

$\Delta G_{DF}$ is commonly called the "driving free energy" for the transformation; it must be negative for the transformation to occur. We call the first term on the right-hand side of (18) the "crystallization free energy", evaluated using (4) and (16a):

$$\Delta G_C = -F_C = X_L \Delta\mu_B + (1 - X_L)\Delta\mu_A; \tag{20}$$

the relationship of $v$ to $\Delta G_C$ is the subject of assumptions discussed later. The "solute drag free energy" $\Delta G_D$ is evaluated in a sharp interface model by taking the product of the diffusive flux and its conjugate

driving force using (3) and (16b):

$$\Delta G_D = J_D(\Delta\mu_A - \Delta\mu_B)\Omega/v$$
$$= (X_L - X_S)(\Delta\mu_A - \Delta\mu_B). \quad (21)$$

Evaluation of (21) in terms of measurable quantities is straightforward for the dilute solution limit when $\Delta\mu_A \to 0$ and $\Delta\mu_B \to RT \ln k/k_e$:

$$\Delta G_D = -X_S[(1-k)/k]RT \ln[k/k_e(T)]. \quad (22)$$

As we increase the concentration of B, the dilute solution approximation becomes invalid when $X_L$ is no longer negligible in (11) or when activity coefficients are no longer constants. in this more general case, (22) must be replaced by

$$\Delta G_D = -X_S[(1-k)k]RT \ln(k/k_A\kappa_e). \quad (23)$$

Up to this point, we have made several assumptions. We have assumed that the dissipation of free energy at the interface is independent of that in the bulk. We have assumed that the former can be written in terms of products of fluxes across the interface and driving forces evaluated across the interface. We have assumed in equation (9) that the diffusive flux is related to its driving force by a particular form of simple chemical rate theory. Additional dissipation at the interface, such as that due to heat flow, has been ignored [15]. Finally, we have assumed steady-state fluxes on a microscopic scale which, strictly speaking, yields only an estimate to $\Delta G_D$. (In order for this term to be evaluated correctly, e.g. in the stepwise growth model [14], the complete time-dependence of $J_D$ and $F_D$ would have to be known and their product would have to be integrated over time.)

We now require a model for how the growth velocity is related to the free energy terms before equation (18) can be solved for $v$. Here we can insert any model appropriate to the particular transformation and to the particular material under consideration. The result will be a self-consistent set of predictions for the interface response functions. For the purpose of making specific calculations for alloy solidification, we use a common model relating the velocity in a single-component system to the driving force at an atomically "rough" interface growing by a "continuous growth" mechanism [30, 31]. Chemical rate theory is used to treat the growth velocity in a similar manner to the treatment of the solute–solvent redistribution problem above. Individual atoms are assumed to hop back and forth from the liquid to the crystal by thermal activation across a barrier. The model yields

$$v = v_0(T)[1 - \exp(\Delta\mu/RT)], \quad (24)$$

where $v_0$ is the maximum speed of crystal growth at infinite driving force (i.e. when the back reaction vanishes), and $\Delta\mu$ (defined to be negative during solidification) is the free energy difference responsible for interface motion. A noteworthy feature of this particular model is that the velocity is proportional to the driving force for small driving forces. Even in models for first order phase transitions that are fundamentally very different [32], $v$ is proportional to the driving force for small driving forces. For solidification of metallic alloys and other processes in which interface mobilities are very large, the driving forces are usually small compared to $RT$. When appropriate, a parabolic relation, such as is expected for a screw dislocation mechanism of solidification [33], might be used instead. For our purposes, the exact form of the velocity-driving force relation is not important, provided that it is not too pathological.

To apply this model to alloys, some averaging must be done. We assume that we can describe the alloy kinetics in terms of hopping across a similar barrier, but of course when there are two species the driving forces in the two cases are different, and the barriers can in principle also be different. Treating them independently and summing their fluxes to find the net crystal growth rate [7] does not yield solute trapping. Even if some coupling is built into the rate equations [13], solute trapping does not result on both sides of a phase diagram [34]. We have therefore gone to the other extreme and expressed the solidification reaction as one of complete dependence, where we imagine the solute and solvent atoms crystallizing as a molecule. With this point of view, $v_0$ in (24) is an average characteristic velocity for the growth reaction.

There are many ways to extend this model to alloys and obtain qualitatively reasonable results. We investigate two of them below. We assume that a modified free energy difference responsible for interface motion enters into equation (24) in the same way that $\Delta\mu$ does in pure materials. This modified free energy difference can be $\Delta G_{DF}$ [14, 35], which represents the entire free energy dissipated at the interface. This assumption yields

$$v = v_0[1 - \exp(\Delta G_{DF}/RT)]. \quad (25)$$

(Recall that the free energy differences here are negative quantities during solidification.) This equation is reasonable. An argument in support of (25) is that the crystallization rate should be determined by the driving force for crystallization averaged over all of the atoms that actually crystallize. Another possibility for replacing $\Delta\mu$ in (24) is that some of the overall driving free energy is consumed in driving the solute–solvent redistribution reaction and is therefore unavailable to drive interface motion. That amount is assumed to be exactly $\Delta G_D$. This assumption yields

$$v = v_0[1 - \exp((\Delta G_{DF} - \Delta G_D)/RT)], \quad (26)$$

or, combined with (18),

$$v = v_0[1 - \exp(\Delta G_C/RT)]. \quad (27)$$

This equation is also reasonable. An argument in support of (27) is that the liquid atoms should

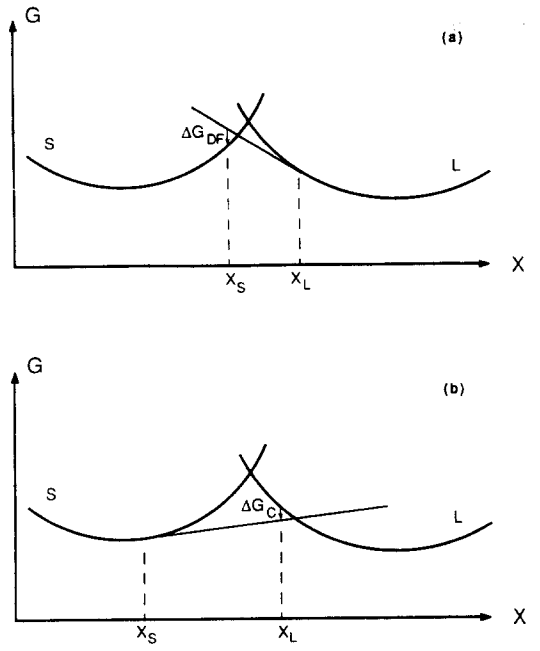


Fig. 2. Construction for obtaining composition of growing solid given temperature and composition of liquid at interface. (a) Model without solute drag, $\Delta G_{DF} \to 0$ as $v_0 \to \infty$. (b) Model with solute drag, $\Delta G_C \to 0$ as $v_0 \to \infty$.

crystallize at a rate determined by the driving force for crystallization averaged over all of the atoms in the liquid at the interface. The model corresponding to equation (25) is denoted "no solute drag" because it does not allow the solute-solvent redistribution reaction to slow down the interface. The model corresponding to equation (27) is denoted "with solute drag". In the linear regime, where the driving forces are small compared to $RT$, (25) becomes $v = -M\Delta G_{DF}$, where $M = v_0/RT$ is conventionally called the mobility of the interface; (27) becomes $v = -M(\Delta G_{DF} - \Delta G_D)$. The alternative to making assumptions about how $\Delta G_{DF}$ is dissipated in driving interface motion seems to require detailed information about the structure, energetics, and atomic mobility throughout the interface. This approach is discussed in the following section.

There is a useful construction involving $\Delta G_{DF}$, $\Delta G_C$, and the free energy curves for the solid and liquid phases, shown in Fig. 2. $\Delta G_{DF}$ is the vertical distance, at composition $X_S$, to the solid curve from the tangent to the liquid curve at $X_L$, as shown in Fig. 2(a). Given a temperature and a liquid composition, one can use these curves to determine the solid composition when $v$ and $v_D$ are small compared to $v_0$. For if $v/v_0$ is very small then in the model without solute drag $\Delta G_{DF}$ is very small in (25). Thus the vertical arrow in Fig. 2(a) is very small. Very little error is involved then in locating the solution to equation (25) by approximating $X_S$ in Fig. 2(a) by the intersection of the solid curve with the tangent from the liquid curve at $X_L$. Likewise, $\Delta G_C$ is the vertical distance, at composition $X_L$, from the liquid curve to the tangent to the solid curve at $X_S$, as shown in Fig. 2(b). In the model with solute drag $\Delta G_C$ is very small in (27); we locate the solution to (27) by approximating $X_S$ in Fig. 2(b) by the point on the solid curve whose tangent intersects the liquid curve at $X_L$. The actual solutions to (25) and (27) lie to the left of the intersections in Figs 2(a) and 2(b), respectively, by amounts that scale with $v/v_0$. Note that these constructions are independent of the particular form of the $k(v)$ equation used. Within the context of this model, we expect the constructions to be quite accurate for materials exhibiting collision-limited growth solidification kinetics, for which $v_0$ should be of the order of the speed of sound. The velocity can then be found by inverting a $k(v)$ equation, such as (11) or (12). The constructions break down by the time $X_L$ crosses the $T_0$ line, the intersection of the two free energy curves. By this point, the arrows in Figs 2(a) and 2(b) must be large enough to be drawn to scale on the diagrams. If $v_D$ is similar in magnitude to $v_0$, then the liquid and solid compositions do not deviate significantly from the local equilibrium compositions until $v$ approaches $v_0$, and the range of validity of the construction is quite limited. Finally, note from the constructions that in the model with solute drag the liquid composition drops with increasing $v$ much faster than the solid composition rises, whereas the reverse is true in the model without solute drag.

## 3. RELATION TO CONTINUUM MODEL

In his original analysis of the solute drag effect, Cahn [36] modelled a grain boundary as two uniform, bulk grains separated by a region of finite width across which the energy of the solute atom varies continuously. He then assumed that the transport of solute across this region is governed by a continuum diffusion equation and solved for the steady-state concentration profile in a moving reference frame. If the energy of the solute is $E(y)$, where $y$ is the distance from the center of the boundary, the boundary exerts a force $-\mathrm{d}E/\mathrm{d}y$ on the solute atom and the solute atom must therefore exert a force $\mathrm{d}E/\mathrm{d}y$ on the boundary. The force, $P$, due to the solute atoms only, per unit area of boundary is therefore the integral of the product of $\mathrm{d}E/\mathrm{d}y$ and the solute concentration, $X(y)/\Omega$, across the boundary. Cahn's analysis was for a dilute solution and he was concerned only with the force due to one species.

Baker and Cahn [11] applied this treatment to motion of interphase boundaries, solving the steady-state diffusion equation across the interface to obtain the velocity dependence of the partition coefficient. They did not evaluate the solute drag in this model. We do this below. The force on the interface due to *both* species in given by

$$P = -(1/\Omega)\int_{-\infty}^{\infty} [X(y)(\mathrm{d}\mu_B'/\mathrm{d}y) + (1 - X(y))(\mathrm{d}\mu_A'/\mathrm{d}y)]\,\mathrm{d}y. \quad (28)$$

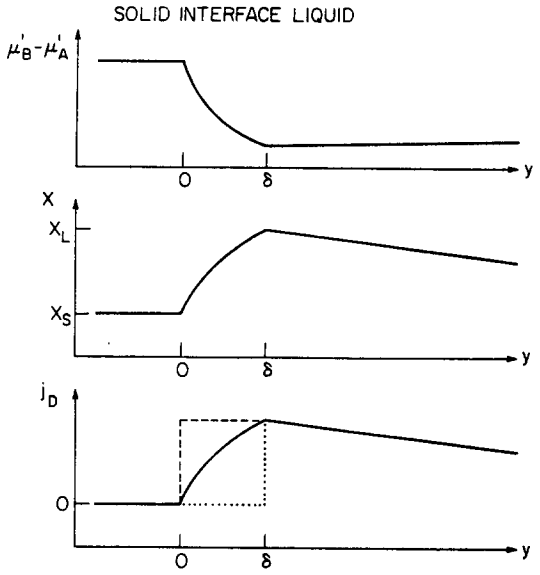


Fig. 3. Potentials, compositions, and fluxes in a continuum model. Variation of solute potential (top) and composition (middle) across the interface. Variation of diffusive flux (bottom) across the interface. Dashed line: diffusive flux corresponding to model "with solute drag"; dotted line: diffusive flux corresponding to model "without solute drag".

where for the general case of a concentrated, non-ideal solution $E$ is replaced by $\mu'$. At this point we will assume no particular functional forms for $\mu_B'(y)$ and $\mu_A'(y)$, but they are assumed to be continuous across the interface, as shown in Fig. 3 (top). With the definition of $\mu'$ as $\mu - RT\ln X$, the above expression can be rewritten in terms of the chemical potentials:

$$P\Omega = -\int_{-\infty}^{\infty} [X(y)(\mathrm{d}\mu_B/\mathrm{d}y) + (1 - X(y))(\mathrm{d}\mu_A/\mathrm{d}y)]\,\mathrm{d}y. \quad (29)$$

The integral in (29) can be broken up into contributions from the two bulk phases plus a contribution from the interface. When gradient energy terms can be neglected, the integrand in each bulk phase vanishes due to the Gibbs–Duhem relation. Integrating across the interface only, we have

$$P\Omega = -\{(1 - X_S)\Delta\mu_A + X_S\Delta\mu_B\} + \int_0^{\delta} \{[X(y) - X_S][\mathrm{d}(\mu_B - \mu_A)/\mathrm{d}y]\}\,\mathrm{d}y. \quad (30)$$

The first term, in curly brackets, is the familiar driving free energy (see equation 19). The remaining integral is the generalized solute drag free energy in the continuum model. Now in the sharp interface model we defined a diffusive flux as $J_D = (v/\Omega)[X_L - X_S]$. In the continuum model, we wish to generalize this concept so that it is defined at all $y$. The flux of B in a coordinate system fixed on the lattice across a plane at arbitrary $y$ is $j_d(y) = (v/\Omega)[X(y) - X_S]$. If the concentration profile is as displayed schematically in Fig. 3 (middle), then $j_d(y)$ is as displayed in Fig. 3 (bottom). Note that $J_D = j_d(\delta)$. Substituting the expression for $j_d(y)$ into (30), we obtain

$$P\Omega = -\Delta G_{DF} + (\Omega/v) \times \int_0^{\delta} j_d(y)[\mathrm{d}(\mu_B - \mu_A)/\mathrm{d}y]\,\mathrm{d}y. \quad (31)$$

By comparison of the above integral with equation (21) we see that the dissipation due to solute–solvent redistribution per unit area of interface per unit time is now given by the product of a *varying* diffusive flux and its conjugate driving force, integrated across the interface.

This integral cannot be evaluated without specific knowledge of $\mu_B'(y)$, $\mu_A'(y)$, and an equation relating the rate of redistribution to the driving force, such as (5).† Baker and Cahn assumed a continuum diffusion equation instead of (5), and chose a family of linear forms for $E(y)$ that facilitated the solution of the diffusion equation. They were able to obtain solutions for an arbitrary degree of impurity adsorption or desorption at the interace. The Baker–Cahn model gives a useful qualitative picture of the transition from equilibrium partitioning to a partitionless transformation. However, the assumed form for $E(y)$ and the use of the continuum diffusion equation produces results for $k(v)$ that are not in quantitative accord with solidification experiments [28]. Without further speculation about the correct rate equation, we can examine two limiting cases for $j_d(y)$ when there is no preferential solute adsorption or desorption at the interface (i.e. the composition lies between $X_L$ and $X_S$ throughout the interface). Suppose that, due to a particular form of $\mu_A'(y)$ and $\mu_B'(y)$ and a particular redistribution rate equation, $j_d$ were constant across the interface and equal to its value at $y = \delta$, as shown by the dashed curve in Fig. 3 (bottom). In this case the integral in (31) can be evaluated readily, yielding

$$P\Omega = -\{(1 - X_S)\Delta\mu_A + X_S\Delta\mu_B\} - (X_L - X_S)(\Delta\mu_B - \Delta\mu_A), \quad (32)$$

or

$$P\Omega = -\Delta G_C, \quad (33)$$

as can be seen by comparison with (20). If, on the other hand, $j_d$ were constant and equal to its value at $y = 0$, as shown by the dotted curve in Fig. 3 (bottom), we would have

$$P\Omega = -(1 - X_S)\Delta\mu_A - X_S\Delta\mu_B = -\Delta G_{DF}. \quad (34)$$

With the further assumption that for small forces on the interface the velocity is proportional to the force, (33) corresponds to (27), the model "with solute drag", and (34) corresponds to (25), the model "with-

†The above expressions can be converted to the more familiar expressions for dilute solutions by replacing $\mu'$ with the standard chemical potential, typically denoted by $\mu$ but denoted by $E$ by Baker and Cahn.

out solute drag". Thus either result appears to be a physically plausible description of a transformation and experiments may be necessary in order to ultimately determine which, if either, model is more appropriate.† Certainly for phase transformations occurring at an atomically sharp interface, we can only define the forces and fluxes in terms of the concentrations on either side of the interface. In this case (33) or (34) may have more validity than (31) in properly describing the interface kinetics.

## 4. RESULTS

In this section we present and compare results of the model "without drag" (equations 11 and 25) and "with drag" (11 and 27). These kinetic models require as input the chemical potential of each species in each phase at all temperatures and compositions of interest. An accurate thermodynamic model is essential if we hope to compare the predictions of any kinetic model with experimental results, for if the predictions do not agree with experiment we must know whether the fault lies in the thermodynamics or in the kinetics. We first present the results of calculations for solidification of a two-component system in which the liquid and the solid are both ideal solutions. Next we present the results of calculations for solidification of a popular thermodynamic model of Ag–Cu, a simple eutectic system in which the terminal phases have the same crystal structure. Ag–Cu has been modeled thermodynamically throughout the undercooled liquid regime [38, 39]. The only free parameters are the two kinetic parameters: the speed of redistribution at infinite driving force $v_D$, and the speed of crystal growth at infinite driving force $v_0$. We assume that the collision-limited growth model describes solidification in these systems, and therefore use an estimate of $v_0/v_D = 100$, independent of composition and temperature (in practice, $v_D$ may depend more strongly on temperature and composition than does $v_0$).‡

The four variables $X_S$, $X_L$, $T$ and $v$ are related by the pair of equations (11) and (25) in the model "without solute drag", or (11) and (27) in the model "with solute drag". We can thus express any pair of variables in terms of the other pair. We display our results in the kinetic interface condition diagrams of Figs 4–6. They show, for example, the interface temperature and solid composition that result if one imposes a certain velocity and liquid composition at the interface. Alternatively, they show the interface temperature and the liquid composition at the interface that result if one imposes a certain velocity and solid composition on the system, as in steady-state welding [40].

The system in Fig. 4 is an ideal solution in both the liquid and the solid. The melting points are 1700 and 100 K; the molar entropy of fusion is taken to be constant at 2.3 R. The dilute solution limit $k_0$ of the equilibrium partition coefficient of B in A is 0.34. The solution of equations (11) and (25) for $v = 0$, displayed as dashed lines in Fig. 4(a), are the solidus and liquidus of the equilibrium phase diagram. The dot-

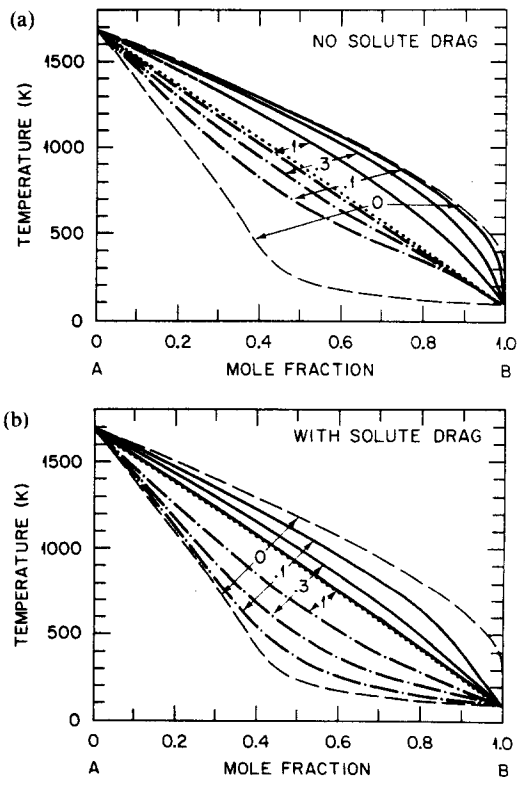


Fig. 4. Kinetic interface condition diagram for ideal solution liquid and solid with melting points as shown, entropy of fusion = 2.3 R, and $v_0/v_D = 100$. (a) Solutions of equations (11) and (25) "without solute drag"; (b) equations (11) and (27) "with solute drag"; for values of $v/v_D$ shown. Dashed lines: solutions for $v = 0$ corresponding to equilibrium phase diagram. Dotted line: $T_0$ curve. Solid line: kinetic liquidus. Dot–dashed line: kinetic solidus.

†This result is to be contrasted with the unproven claim of Caroli *et al.* [37] that (27) is the only reasonable way the free energy can enter into the expression for the growth velocity. In addition, note that these authors are describing a different physical process than we are by the term "solute drag".

‡For the purpose of these calculations, $Q_D$ is defined to be $\mu'$ of the transition state minus the greater value of $\mu'$ of the states on either side of the transition state. With this definition, the assumption that $Q_D$ is a constant across the entire phase diagram results in realistic diffusive fluxes across a nonvanishing barrier, independent of the magnitude or sign of $(\Delta\mu'_B - \Delta\mu'_A)$. Because of this definition, however, (6) and (7) must be replaced, respectively, by

$$J_D^+ = (fv\lambda)(X_S/\Omega)(1 - X_L) \times \exp\{-[Q_D - (\Delta\mu'_B - \Delta\mu'_A)]/RT\} \quad (6')$$

and

$$J_D^- = (fv\lambda)(X_L/\Omega)(1 - X_S)\exp\{-Q_D/RT\}, \quad (7')$$

when $\Delta\mu'_B - \Delta\mu'_A$ is negative, which occurs on the Cu-rich side of the kinetic interface condition diagrams in Figs 5 and 6.

ted line is the $T_0$ curve, which is the locus of the intersections of the solid and liquid free energy curves in Fig. 2; it represents the maximum temperature at which a solid of a given composition can be formed from a liquid of any composition. The solid and dot–dashed curves labelled ".1" in Fig. 4(a) are the "kinetic" liquidus and solidus (solutions to the equations) for an imposed interface speed of 0.1 $v_D$. The liquidus and solidus begin to approach each other, reflecting the increasing partition coefficient (which is the ratio of the kinetic solidus and liquidus compositions). The curves labelled ".3" and "1" are the solutions for $v = 0.3\, v_D$ and $v = v_D$ respectively. As $v$ increases, the kinetic solidus initially rises toward the $T_0$ line more rapidly than the kinetic liquidus drops, as predicted by the construction in Fig. 2(a). As the velocity increases beyond $v_D$ (not shown), the undercooling increases further while the kinetic liquidus and solidus merge ($k \to 1$).

In Fig. 4(b) are plotted the solutions to equations (11) and (27) for the same conditions as in Fig. 4(a). We see that in the formulation "with solute drag", the kinetic liquidus approaches the $T_0$ line more rapidly than does the kinetic solidus [compare Figs 4(b) and 2(b)]. Eventually, of course, the kinetic solidus and liquidus merge and the interface temperature drops as $v$ exceeds $v_D$.

If several solid phases with different crystal structures can grow from the melt then separate solutions must be obtained for each structure. In such a case, the resulting kinetic interface condition diagram is obtained by superposition of one simple diagram [such as Fig. 4(a)] for each structure. For example, solidification in a simple eutectic system in which the terminal phases have different crystal structures might be described by a superposition of Fig. 4(a) on its mirror image. The model presented in this paper does not predict which phase will actually be observed.

In Figs 5 and 6 we show the solutions to equations (11) and (25), and (11) and (27), respectively, for Murray's thermodynamic model of the Ag–Cu system [38]. Again we assume $v_0/v_D = 100$. The equilibrium solidi and liquidi are again denoted by dashed curves and the $T_0$ curve is dotted. Solid–solid equilibrium below the eutectic has been omitted; metastable solid–liquid equilibria are depicted instead. The solid and dot-dashed curves in Fig. 5(a) are the kinetic liquidus and solidus solutions to equations (11) and (25) "without solute drag" for an imposed interface speed of 0.01 $v_D$. At this speed, the kinetic liquidus has not yet moved noticeably but the kinetic solidus has already moved in somewhat. Multiple solutions are found in the middle of the diagram. This region of the phase diagram lies under the chemical spinodal for the solid and may therefore be unobservable experimentally. Since our treatment neglects effects such as coherency strain that tend to stabilize the solid against spinodal decomposition, we have included these solutions in the event that some of them might be realized experimentally. Note that Duwez and coworkers apparently produced Ag–Cu solid solutions across the entire phase disgram by splat quenching [41]. Note also that strictly speaking the solutions are for a planar interface only, whereas experimental conditions may often result in cellular or dendritic breakdown of the interface in this region of the phase diagram. However, for first-order phase transitions such relations yield reasonable results for a curved interface if the driving free energy is modified by a capillarity term [12]. In Fig. 5(b) we plot the solutions for an imposed interface speed of 0.1 $v_D$. As the interface speed is increased further to 0.7 $v_D$ [Fig. 5(c)], the kinetic solidus approaches the $T_0$ curve and $k$ approaches unity. The kinetic liquidus and solidus merge and the transformation becomes virtually partitionless at $v = 30\, v_D$ [Fig. 5(d)].

The interface condition diagrams are quite different if we use (27), in which we subtract off the solute drag, rather than (25). In Fig. 6(a) we show the numerical solutions of equations (11) and (27) for an imposed interface speed of 0.1 $v_D$. The already substantial undercooling of the kinetic liquidus below the equilibrium liquidus is due almost entirely to the solute drag term. In Fig. 6(b) we plot the solutions for an interface speed of 0.3 $v_D$. Representative tie-lines are shown to aid the reading of the diagrams. At this speed, the kinetic liquidus is approaching the $T_0$ curve as the degree of solute trapping and of interfacial undercooling increase. At $v = 3\, v_D$ [Fig. 6(c)], the solute drag term is rapidly disappearing. This conclusion can be drawn by comparing the undercooling in the middle of the diagram to that of pure Ag and pure Cu at the two ends of the diagram, where the solute drag term is identically zero. Note that at this speed a partitionless transformation is thermodynamically possible but, however, does not occur until still greater speeds, where the kinetic solidus and liquidus merge and become completely indistinguishable [Fig. 5(d)].

In the model "with solute drag", significantly more undercooling is predicted than without solute drag. The difference between the predicted undercoolings in the two models is evident at $v/v_D = 0.1$ [Figs 6(a) and 5(b)]. This behavior can be understood in the context of Fig. 2. Note how close the kinetic solidus lies to $T_0$ at $v/v_D = 0.7$ [Fig. 5(c)] in the model without solute drag, compared to the proximity of the kinetic liquidus and $T_0$ at $v/v_D = 0.3$ [Fig. 6(b)] when solute drag is included.

An instability in the steady-state solution occurs where a tie line connects a kinetic solidus and a kinetic liquidus having opposite slopes, such as in the central regions of Figs 5(a) and (b) and 6(a) and (b). A fluctuation whereby a small amount of crystal grows with more solute than the steady-state amount will make the liquid at the interface leaner in solute, thus shifting the steady-state kinetic solidus solution to yet greater solute concentrations. The unstable branches of the kinetic solidi and liquidi are denoted

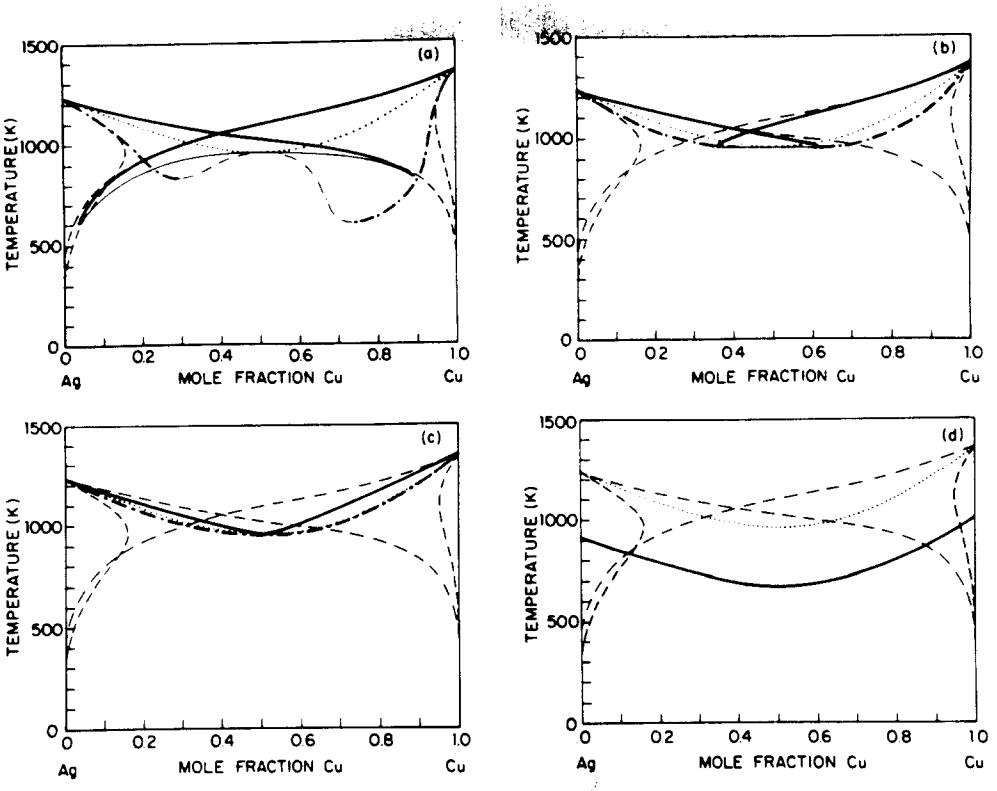


Fig. 5. Kinetic interface condition diagram "without solute drag" for Ag–Cu assuming $v_0/v_D = 100$ and equations (11) and (25). Solute drag is not subtracted off of the driving free energy before the latter is employed to move the interface. Dashed lines: equilibrium solidus and liquidus. Dotted line: $T_0$ curve. Solutions for: (a) $v/v_D = 0.01$; solid line: kinetic liquidus; dot–dash line: kinetic solidus. Thin regions of kinetic solidus and liquidus denote unstable roots; (b) $v/v_D = 0.1$; (c) $v/v_D = 0.7$; (d) $v/v_D = 30$.

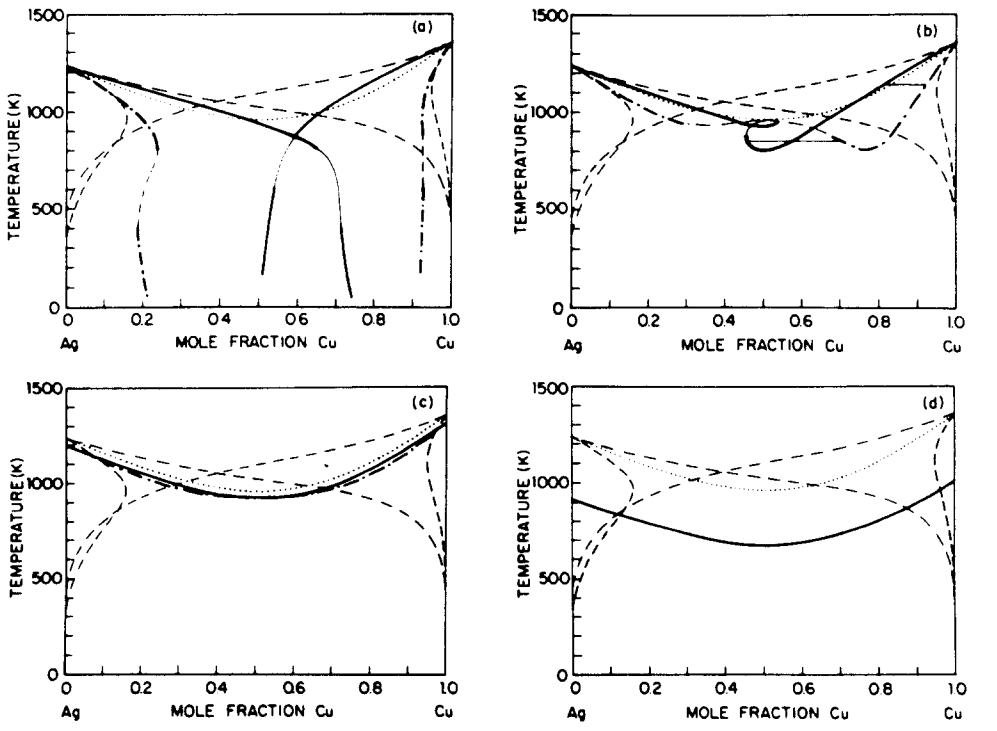


Fig. 6. Kinetic interface condition diagram "with solute drag" for Ag–Cu assuming equations (11) and (27). Solutions with $v_0/v_D = 100$ for: (a) $v/v_D = 0.1$; (b) $v/v_D = 0.3$, horizontal lines are tie lines; (c) $v/v_D = 3$; (d) $v/v_D = 30$.

by thin lines in Figs 5 and 6. This effect could give rise to oscillatory behavior when a constant solidification velocity is imposed on material with a bulk liquid composition in this region [42]. Strictly speaking, the models presented in this paper yield steady-state response functions only, and any oscillatory behavior cannot be described in terms of such roots. However, we expect the time it takes for the interface to reach a "steady-state" configuration to be rather short, on the order of $\delta^2/D_i$, where $\delta$ is the width of the interface. Thus a steady state model may adequately describe unsteady behavior also.

During rapid solidification following pulsed laser melting of semiconductors, the interface has been observed to slow down upon encountering a heavily doped region [43, 44]. The interface velocity was measured in these experiments by observing rapid changes in the transverse electrical conductance of a thin film specimen as the phase transformation proceeds [3, 45]. Whether the observed interface slowdown is mainly due to solute drag, a reduced driving force for solidification, or a reduced interface mobility remains to be seen. This transient conductance technique has recently been successfully applied to metallic thin films [46] as well. In the near future, experiments of this type may enable us to make quantitative tests of models for the interface velocity vs undercooling and composition response functon.

## 5. SUMMARY

A model has been developed for the two response functions of a planar interface in a two-component system and applied to alloy solidification.

The CGM solute trapping model, which has received some experimental support, has been employed for the solute partitioning response function.

The velocity-driving force response function is developed by generalizing the chemical potential difference in a velocity-vs-driving free energy function that is commonly used for solidification of one-component melts. Two different ways of generalizing the chemical potential difference are used. In the first, denoted "without solute drag", the chemical potential difference is replaced by the free energy change upon solidification of one mole of alloy, resulting in:

$$v = v_0[1 - \exp(\Delta G_{DF}/RT)].$$

In the second, denoted "with solute drag", some of this driving free energy is assigned to drive solute-solvent redistribution across the interface and is considered to be unavailable for driving interface motion. The result is

$$v = v_0[1 - \exp((\Delta G_{DF} - \Delta G_D)/RT)].$$

These two versions of the model are shown to be limiting cases of the continuum model of Baker and Cahn.

The results have been presented in kinetic interface condition diagrams, which reproduce the equilibrium phase diagram at zero velocity and depict interfacial undercooling and suppressed solute partitioning as the interface speed increases. Predictions have been made for an ideal solution and for a simple eutectic system in which the terminal phases have the same crystal structure.

Results have been presented both with and without solute drag. If free energy dissipation due to solute drag is not explicitly subtracted from the driving free energy before the latter is employed to drive interface motion, substantially less interfacial undercooling is predicted than otherwise.

*Acknowledgements*—We thank J. W. Cahn and W. J. Boettinger for much helpful discussion. One of us (M.J.A.) was supported in part by an appointment to the U.S. Department of Energy Faculty Research Participation Program administered by Oak Ridge Associated Universities. Work at Harvard was supported by the Harvard Materials Research Laboratory under NSF contract DMR-83-16979. Work in Oak Ridge was supported by the Division of Materials Sciences, U.S. Department of Energy under contract DE-AC05-84OR21400.

## REFERENCES

1. J. C. Baker and J. W. Cahn, in *Solidification*, p. 23. American Soc. for Metals, Metals Park (1970).
2. W. J. Boettinger, in *Rapidly Solidified Amorphous and Crystalline Alloys* (edited by B. H. Kear and B. C. Giessen). Elsevier/North Holland, New York (1982).
3. M. O. Thompson, J. W. Mayer, A. G. Cullis, H. C. Webber, N. G. Chew, J. M. Poate and D. C. Jacobson, *Phys. Rev. Lett.* **50**, 896 (1983).
4. J. C. Baker and J. W. Cahn, *Acta metall.* **17**, 575 (1969).
5. C. W. White, S. R. Wilson, B. R. Appleton and F. W. Young Jr, *J. Appl. Phys.* **51**, 738 (1980).
6. P. Baeri, J. M. Poate, S. U. Campisano, G. Foti, E. Rimini and A. G. Cullis, *Appl. Phys. Lett.* **37**, 912 (1980).
7. K. A. Jackson, *Can. J. Phys.* **36**, 683 (1958).
8. R. N. Hall, *J. Phys. Chem.* **57**, 836 (1953).
9. A. A. Chernov, in *Growth of Crystals*, vol. 3 (edited by A. V. Shubnikov and N. N. Sheftal), p. 35. Consultants Bureau, New York (1962).
10. J. C. Brice, *The Growth of Crystals from the Melt*, p. 65. North-Holland, Amsterdam (1965).
11. J. W. Cahn, S. R. Coriell and W. J. Boettinger, in *Laser and Electron Beam Processing of Materials* (edited by C. W. White and P. S. Peercy), p. 89. Academic Press, New York (1980).
12. M. Hillert and B. Sundman, *Acta metall.* **25**, 11 (1977).
13. K. A. Jackson, in *Surface Modification and Alloying by Laser, Ion and Electron Beams* (edited by J. M. Poate, G. Foti and D. C. Jacobson), p. 51, Plenum Press, New York (1983).
14. M. J. Aziz, *J. Appl. Phys.* **53**, 1158 (1982).
15. M. J. Aziz, *Appl. Phys. Lett.* **43**, 552 (1983).
16. G. H. Gilmer, *Mater. Res. Soc. Symp. Res.* **13**, 249 (1983).
17. R. F. Wood, *Appl. Phys. Lett.* **37**, 302 (1980).
18. M. J. Aziz, J. Y. Tsao, M. O. Thompson, P. S. Peercy and C. W. White, *Mater. Res. Soc. Symp. Proc.* **35**, 153 (1985).
19. M. J. Aziz and C. W. White, *Phys. Rev. Lett.* **57**, 2675 (1986).

20. M. J. Aziz, in *Laser Surface Treatment of Metals* (edited by C. W. Draper and P. Mazzoldi), p. 649. Nijhoff, Dordecht (1986).
21. D. Turnbull, in *Thermodynamics in Physical Metallurgy*, p. 282. American Soc. for Metals, Cleveland (1950).
22. G. H. Vineyard, *J. Phys. Chem. Solids* **3,** 121 (1957).
23. D. Turnbull, *J. phys. Chem.* **66,** 609 (1962).
24. S. R. Coriell and D. Turnbull, *Acta metall.* **30,** 2135 (1982).
25. J. W. Christian, *Theory of Transformations in Metals and Alloys*, 2nd edn, Part I, Chapter 4. Pergamon Press, Oxford (1975).
26. R. F. Sekerka and W. W. Mullins, *J. chem. Phys.* **73,** 1413 (1980).
27. A. C. Smith, J. F. Janak and R. B. Adler, *Electronic Conduction in Solids*, Chapter 2. McGraw-Hill, New York (1967).
28. M. J. Aziz, J. Y. Tsao, M. O. Thompson, P. S. Peercy and C. W. White, *Phys. Rev. Lett.* **56,** 2489 (1986).
29. M. Hillert and B. Sundman, *Acta metall.* **24,** 731 (1976).
30. D. Turnbull, *J. phys. Chem.* **66,** 609 (1962).
31. Ref. [25], p. 479.
32. S.-K. Cahn, *J. chem. Phys.* **67,** 5755 (1977).
33. W. B. Hillig and D. Turnbull *J. chem. Phys.* **24,** 914 (1956).
34. M. J. Aziz, J. Y. Tsao, M. O. Thompson, P. S. Peercy, C. W. White and W. H. Christie, *Mater. Res. Soc. Symp. Proc.* **35,** 153 (1985).
35. W. J. Boettinger, S. R. Coriell and R. F. Sekerka, *Mater. Sci. Engng* **65,** 27 (1984).
36. J. W. Cahn, *Acta metall.* **10,** 789 (1962).
37. B. Caroli, C. Caroli and B. Roulet, *Acta metall.* **34,** 1867 (1986).
38. J. L. Murray, *Metall. Trans.* **A15,** 261 (1984).
39. D. G. Beck, S. M. Copley and M. Bass, *Metall. Trans.* **A13,** 1879 (1982).
40. W. J. Boettinger, D. Shechtman, R. J. Schaefer and F. Biancaniello, *Metall. Trans.* **A15,** 55 (1984).
41. P. Duwez, R. H. Willens and W. Klement, *J. appl. Phys.* **31,** 1136 (1960).
42. M. J. Aziz, in *Undercooled Alloy Phases* (edited by E. W. Collings and C. C. Koch), p. 390. TMS-AIME, Warrendale, Pa. (1987).
43. G. J. Galvin, J. W. Mayer and P. S. Peercy, *Mater. Res. Soc. Symp. Proc.* **23,** 111 (1984).
44. P. S. Peercy and M. O. Thompson, *Mater. Res. Soc. Symp. Proc.* **35,** 53 (1985).
45. M. O. Thompson, G. J. Galvin, J. W. Mayer, P. S. Peercy and R. B. Hammond, *Appl. Phys. Lett.* **42,** 445 (1983).
46. J. Y. Tsao, S. T. Picraux, P. S. Peercy and M. O. Thompson, *Appl. Phys. Lett.* 48, 278 (1986).